




High-precision anomalous dimension of three-dimensional percolation and spatial profile of the critical giant cluster

Alessandro Galvani ¹, Andrea Trombettoni ^{2,1} and Giacomo Gori ^{3,4}¹SISSA and INFN, Sezione di Trieste, Via Bonomea 265, I-34136 Trieste, Italy²Department of Physics, University of Trieste, Strada Costiera 11, I-34151 Trieste, Italy³Institut für Theoretische Physik, Universität Heidelberg, D-69120 Heidelberg, Germany⁴CNR-IOM DEMOCRITOS Simulation Center and SISSA, Via Bonomea 265, I-34136 Trieste, Italy

(Received 11 November 2021; revised 23 May 2022; accepted 14 November 2022; published 7 December 2022)

In three-dimensional percolation, we apply and test the critical geometry approach for bounded critical phenomena based on the fractional Yamabe equation. The method predicts the functional shape of the order parameter profile ϕ , which is obtained by raising the solution of the Yamabe equation to the scaling dimension Δ_ϕ . The latter can be fixed from outcomes of numerical simulations, from which we obtain $\Delta_\phi = 0.47846(71)$ and the corresponding value of the anomalous dimension $\eta = -0.0431(14)$. The comparison with values of η determined by using scaling relations is discussed. A test of hyperscaling is also performed.

DOI: [10.1103/PhysRevE.106.064111](https://doi.org/10.1103/PhysRevE.106.064111)

I. INTRODUCTION

Percolation describes the addition of links to system leading to the formation of a macroscopic cluster. Despite its simplicity, it can model vastly different real-world phenomena [1], ranging from water passing through coffee to molecules branching to form a gel [2,3] or from wildfires [4] to the spread of infections [5–7].

Percolation provides a clear introduction to critical phenomena, with an easily identifiable transition and a visually striking example of self-similarity at the critical point [8]. It differs from spin systems as it lacks a Hamiltonian, making it an easy to simulate, purely geometrical model. It has been the subject of several physical studies, via methods such as the renormalization group [9–11], as well as boasting a long history of mathematical investigations [12], culminating in a Fields medal [13,14]. The richness of the field is reflected in the variety of related universality classes, including directed [15,16], long-range [5,17–19], and history-dependent [20] percolation, and by the different models within the same class, such as bond or site percolation. Several exact results, including critical exponents, are available in two dimensions [21–24].

At the critical point, percolation is described by a logarithmic conformal field theory [25], with a single primary field [26]. Bond percolation can be obtained as the analytic continuation of the q -state Potts model for $q \rightarrow 1$ [27]; this procedure, however, does not preserve unitarity. For this reason, the most accurate technique currently available to obtain critical exponents for $O(N)$ models, the conformal bootstrap [28], cannot be straightforwardly applied to percolation, meaning that results for anomalous dimensions are not especially precise.

In this work, we apply the geometric theory of bounded critical phenomena introduced in [29] to the case of three-

dimensional (3D) continuum (i.e., off-lattice) percolation. The procedure consists in (1) slicing the giant cluster (defined below) emerging at the critical point, (2) measuring the fraction of the giant cluster at a given distance from the boundaries (similarly to what was done for a discrete two-dimensional (2D) strip in [24]), and (3) comparing it with the solutions of the fractional equation obtained in the critical geometry approach of [29], to extract the scaling dimension Δ_ϕ of the order parameter.

II. CRITICAL GEOMETRY

The main property a system typically gains at its critical points is conformal invariance [30,31]. Heuristically, this means that every region of the system looks the same; introducing a boundary clearly breaks this property. The question addressed in [29] is then: is there a way to recover some degree of uniformity?

To answer this, [29] presents a conjecture, called *uniformization hypothesis*, which is at the heart of the critical geometry approach. According to it, the metric must make a bounded critical system as uniform as possible, by making the scalar curvature constant. This curvature would have to be negative, since spaces with positive curvature, like spheres, lack boundaries.

Starting from the uniformization hypothesis, for models at their upper critical dimension $d = d_c$ [29,32], one can write the requirement of constant scalar curvature as an equation for a factor $\gamma(\mathbf{x})$, obtaining what in geometry literature is called the Yamabe equation [33]:

$$(-\Delta)\gamma(\mathbf{x})^{-\frac{d-2}{2}} = -\frac{d(d-2)}{4}\gamma(\mathbf{x})^{-\frac{d+2}{2}} \quad (1)$$

(Δ is the Laplacian in flat space). With the condition $\gamma(\mathbf{x}) = 0$ at the boundaries of the domain Ω , one obtains

solutions which, close to the boundary, are proportional to the Euclidean distance from it.

For $d < d_c$, to be consistent with the uniformization hypothesis one has to modify the Yamabe equation in order to account for the anomalous dimension η of the field [29]

$$\Delta_\phi = \frac{d - 2 + \eta}{2}. \quad (2)$$

Dimensional analysis suggests that the exponents in (1) be altered: the Laplacian is then replaced by a fractional derivative, leading to

$$(-\Delta)^{d/2 - \Delta_\phi} \gamma_{(\Delta_\phi)}(\mathbf{x})^{-\Delta_\phi} \propto \gamma_{(\Delta_\phi)}(\mathbf{x})^{-d + \Delta_\phi}. \quad (3)$$

Equation (3) is called fractional Yamabe equation [34] for the function $\gamma_{(\Delta_\phi)}(\mathbf{x})$ to be determined. The fractional Laplacian $(-\Delta)^s$ in (3) is a nonlocal operator with many possible definitions [35]. For our purposes, it must be computed through an extension to a $(d + 1)$ -dimensional space, as introduced in [36].

The uniformization hypothesis is an unproven conjecture. If from one side it would be highly desirable to derive it from accepted principles, such as conformal invariance, it does produce testable predictions for correlation functions and in particular for the order parameter profile at criticality. Indeed, once $\gamma(\mathbf{x})$ is known, one-point functions are determined up to a constant α :

$$\langle \phi(\mathbf{x}) \rangle = \frac{\alpha}{\gamma(\mathbf{x})^{\Delta_\phi}}. \quad (4)$$

This prediction for the order parameter correlation function has been shown to hold numerically, with high precision, in [29] for the 3D Ising model, in [32] for the four-dimensional Ising model, and in [37] for the 3D XY model. Uniformization also reproduces known 2D results [29].

Percolation offers the possibility to use and test the critical geometry approach: from one side, if one assumes the value of η available in literature, then Eq. (4) gives predictions for the spatial profile of the order parameter at criticality, which are not easy to provide for percolation in dimension larger than two with other approaches. From the other side, for percolation in $d = 3$ the exponent η is known with much lower precision than the corresponding exponent in other models, such as the Ising model [38]. So a truly challenging task for the critical geometry approach is to determine η for 3D percolation with high precision. Once direct determinations of η become available, they would provide a stringent test for critical geometry. Moreover, the current high precision estimates of η obtained with scaling relations already provide a good test for our approach. Independently from this test, checking scaling and hyperscaling relations using the values of the other critical exponents also puts a bound on the validity of the critical geometry approach. At the same time, one obtains in this way as a by-product predictions for the critical order parameter profile.

III. ORDER PARAMETER PROFILE

The idea is to solve the fractional Yamabe equation in the considered domain and use the solution to find the order parameter profile. Fitting the profile of the order parameter with numerical data will give us the value of the scaling

dimension Δ_ϕ . For a spin model, the order parameter $\langle \phi(\mathbf{x}) \rangle$ is the magnetization, while for percolation it can be extracted by a slicing procedure performed on the giant cluster. We choose the geometry of a slab, with $\gamma(\mathbf{x})$ depending only on the transverse direction, where we denote by $\mathbf{x} = (x, \mathbf{y})$ the points on the slab, with $x \in [0, L]$ and $\mathbf{y} \in [0, L']^{d-1}$.

It is instructive to apply this method for $d = 2$, where exact results are known [39]. Taking the $d \rightarrow 2$ limit to the Yamabe equation (1), one gets the Liouville equation:

$$(-\Delta) \log \gamma(\mathbf{x}) = -\gamma(\mathbf{x})^{-2}. \quad (5)$$

In two dimensions a metric is entirely defined by its scalar curvature: the solution of the Liouville equation also solves the fractional Yamabe equation for any Δ_ϕ [29]. In particular, for a strip of width L for $x \in [0, L]$, $\gamma(x) = \frac{L}{\pi} \sin \frac{\pi x}{L}$.

IV. CONTINUUM PERCOLATION

The discussed approach could be applied to simulation of lattice percolation at the critical point. However, since this approach uses as input continuous order parameter profiles at criticality, it is advantageous to extract these profiles from simulations performed with objects placed continuously in space [40–42], which is commonly referred to as continuum percolation [12]. The algorithm is straightforward: d -dimensional balls with unit diameter are generated, one at a time. The center of each is picked randomly, with uniform probability within a slab. If the ball intersects another one, it is added to the cluster of the latter. If it intersects two or more balls belonging to different clusters, the clusters are merged, as explained in Appendix B. We stop adding objects once the product of their number and the relative volume of one object reaches the critical filling fraction η_c , which means we are at the critical point: measurements can then begin.

The order parameter $\langle \phi(x) \rangle$ is the density of the giant cluster, function of the distance from one boundary parametrized by x . What we call “giant cluster” is the set of all clusters which intersect one or both boundaries (the green balls of Fig. 1); it includes of course the percolating cluster(s) connecting the boundaries. In practice, this means imposing from the start that the two boundaries belong to the same macroscopic cluster. This corresponds to imposing fixed boundary conditions, i.e., diverging order parameter at the boundaries.

The order parameter at a point x is obtained by slicing the giant cluster with a plane, a distance x from one boundary, and then measuring the total area (in two dimensions, length) obtained as intersections between the objects and the plane. This means that the profiles generated by the simulations are continuous themselves, lifting discretization effects (finite-size effects being of course still present).

V. 2D PERCOLATION

Before venturing into the 3D case, we checked that in two dimensions the method gives a value for the exponent Δ_ϕ in agreement with the analytical prediction.

The system is a strip of sizes (in units of the diameter of a sphere) L in the transverse direction x and $4L$ in the parallel direction y , along which periodic boundary conditions

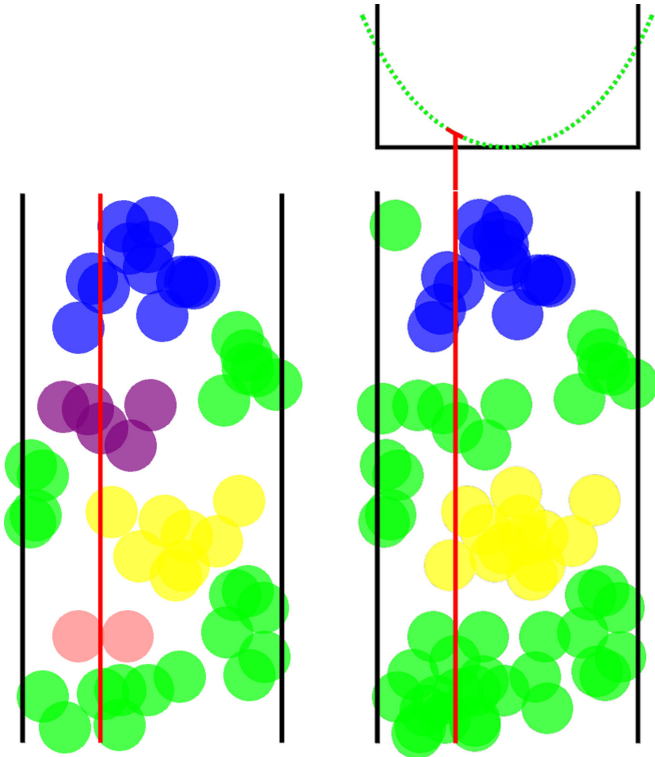


FIG. 1. Continuum percolation in two dimensions. Fixed boundary conditions are enforced: when a circle intersects either boundary, it gets added to the giant cluster (green). Left: $\eta < \eta_c$ – Right: $\eta = \eta_c$. The segments obtained as an intersection between the red line and the green balls contribute to the profile sketched above, obtained by averaging different realizations. The dashed line illustrates the average on different realizations, as shown by the data plotted in Fig. 2; it extends beyond the slab boundaries to illustrate the effect of the extrapolation length a .

are imposed.¹ L ranges from 16 to 128, in steps of eight. The critical filling ratio we used [41] is $\eta_c^{2d} = 1.12808737$ (the error on η_c does not meaningfully alter our results, as seen in Appendix C). Continuous percolation allows us to get comparable results for different sizes, by measuring the order parameter $\langle\phi(x)\rangle$ across a fixed odd number $2n - 1$ of planes for every system size (even for small L), equally spaced throughout the slab. By symmetry, the values x and $L - x$ have been averaged: each profile consists of n points.

Assuming the validity of (4), we fit the order parameter profiles with the function

$$\langle\phi(x)\rangle = \alpha \left[L \gamma_{(\Delta_\phi)} \left(\frac{x}{1 + a/L} \right) \right]^{-\Delta_\phi}, \quad (6)$$

where the fit parameters are a multiplicative constant α , the extrapolation length a (accounting for the fact that the numerical profile does not diverge on the boundary [43]) and the scaling dimension Δ_ϕ .

Once the profiles for different sizes have been rescaled by multiplying each by $L^{-\Delta_\phi}$ and by plotting them as a func-

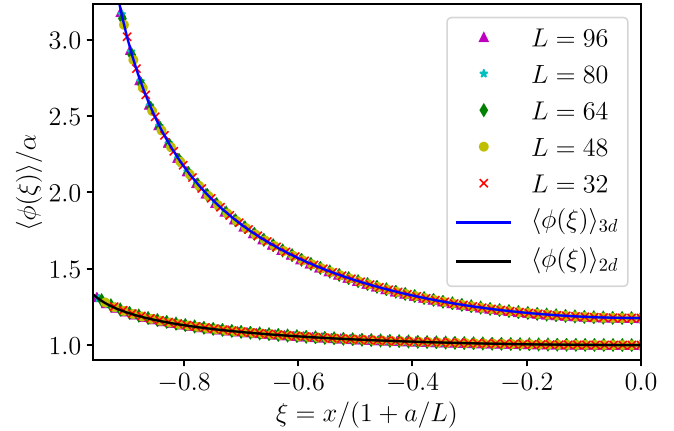


FIG. 2. Order parameter profile for selected sizes, in $d = 2, 3$. We see a clear collapse of the points for different sizes, proving that we are at the critical point. The theoretical curves fit the data points accurately.

tion of $\xi = x/(1 + a_L/L)$, they collapse onto the same curve, $\alpha/\gamma(\xi)^{\Delta_\phi}$, as seen in Fig. 2; each size gives a corresponding $\Delta_\phi(L)$.

We notice in Fig. 3 a decay of the fit parameter $\Delta_\phi^{(2d)}(L)$ as the size L increases. To extrapolate the correct value, free of finite-size effects, we perform a fit in the form of a power law:

$$\Delta_\phi(L) = \frac{c}{L^k} + \Delta_\phi^\infty, \quad (7)$$

with c, k , and Δ_ϕ^∞ as fit parameters. This gives $\Delta_\phi^\infty = 0.1041(5)$, a good estimate, relative to the small numerical effort, of the exact value $\Delta_\phi^{(2d)} = 5/48 \approx 0.10417$.

VI. 3D PERCOLATION

The same can now be done for a 3D slab, as seen in Fig. 4, of sizes $L \times 4L \times 4L$; L ranges from 16 to 100 in steps of four, and the critical filling fraction used is $\eta_c^{3d} = 0.341888$,

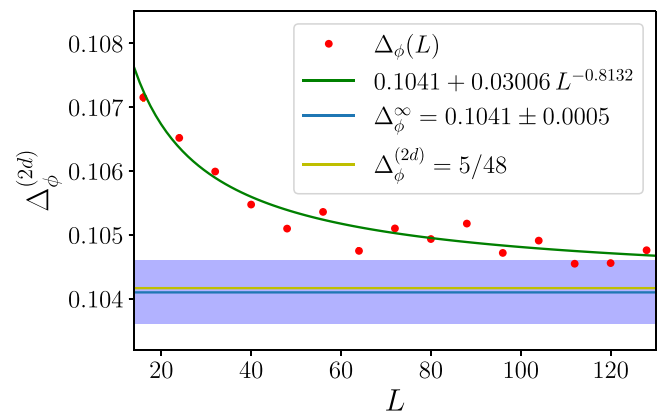


FIG. 3. Fit results $\Delta_\phi(L)$ as the system size L increases in $d = 2$ (red dots). The green line is the extrapolation fitting function (7), while the blue line is our best estimate Δ_ϕ^∞ with the shading representing the error σ on Δ_ϕ^∞ . The yellow line is the exact value. Despite relatively small system sizes, Δ_ϕ^∞ is convincingly close to the exact value.

¹Different ratios between the two sizes have been tested: increasing this ratio beyond 4 does not alter the results.

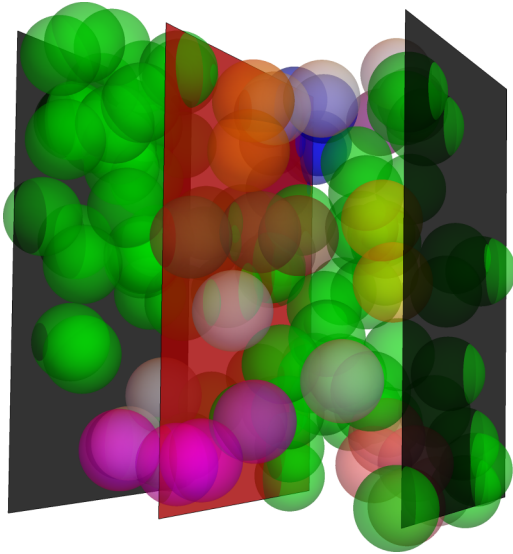


FIG. 4. Giant cluster (green spheres) sliced by a plane (red). The black planes are the system boundaries: balls intersecting either belong to the giant cluster.

currently the most precise estimate [44]. An important difference with respect to the 2D case is the dependence of the fractional Yamabe equation on Δ_ϕ . We thus obtained a solution $\gamma_{(\Delta_\phi)}(x)$ that varies smoothly for $\Delta_\phi \in [0.46, 0.5]$, which includes the correct value. Since $\gamma_{(\Delta_\phi)}$ is almost constant in that range, using the integer Yamabe equation (corresponding to $\Delta_\phi = 1/2$) would be a reasonable initial approximation; Appendix A highlights the difference between the integer and the fractional solutions.

We obtain another clear collapse of the profiles in Fig. 2. The data are indeed described in an excellent way by the fitting function (6). For each system size values of Δ_ϕ are obtained. Similarly to the 2D case a slight decay with L (Fig. 5) is observed. By using a similar infinite-size extrapolation (7) we obtain our estimate for the scaling dimension:

$$\Delta_\phi = 0.47846(71), \tag{8}$$

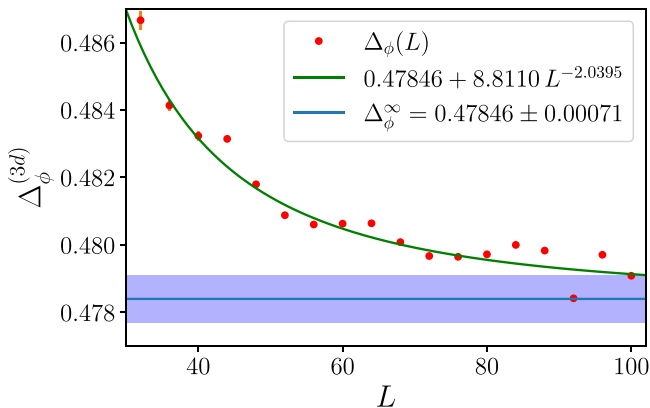


FIG. 5. Finite size estimates $\Delta_\phi(L)$ for the $d = 3$ slab (red dots) as a function of L . The extrapolation curve (7) is the continuous green line, while the infinite size value Δ_ϕ^∞ is the dashed blue line. The shaded area represents the error σ on Δ_ϕ^∞ .

TABLE I. Comparison of the value of the anomalous dimension obtained with various methods. The results above the solid line make use of hyperscaling equalities in different ways: [45] uses (10) but determines ν through a hyperscaling relation involving β ; [50] and [51] determine the Fisher exponent τ , related to the size distribution of clusters, and relate it to η through the fractal dimension d_f , while [46] measures d_f directly. From that one gets η using $\eta = 2 + d - 2d_f$; [49] determines η using the scaling relation (10). Below the dashed line are direct determinations of η using loop expansions [52,53] and our result.

Reference	Year	Method	η
Adler <i>et al.</i> [45]	1990	Moment expansion	$-0.07(5)$
Lorenz and Ziff [50]	1998	MC, bond percolation	$-0.046(8)$
Jan and Stauffer [51]	1998	MC, site percolation	$-0.059(9)$
Xu <i>et al.</i> [46]	2013	MC, multiple lattices	$-0.0458(2)$
Ballesteros <i>et al.</i> [49]	1999	MC, site percolation	$-0.04602(34)$
Gracey [52]	2015	Four-loop RG	-0.0470
Borinsky <i>et al.</i> [53]	2021	Five-loop RG	$-0.06(10)$
This work	2022	Critical geometry	$-0.0431(14)$

where the uncertainty is the statistical error on the fit parameter. From the definition (2), we get the corresponding anomalous dimension:

$$\eta = -0.0431(14). \tag{9}$$

This value is more precise than previous direct determinations of η using other methods, listed in Table I. Future high-precision determinations of η , using different methods, could give further support to the validity of the uniformization hypothesis if compatible, or disprove it if not.

A. Scaling relations

Critical exponents are connected by well-known scaling relations [43], which we can exploit to check the validity of our result. The scaling relation involving η and independent from d is

$$(2 - \eta)\nu = \gamma; \tag{10}$$

substituting our result for η , alongside $\gamma = 1.805(20)$ [45] and $\nu = 0.8762(12)$ [46], we get $1.790(2) = 1.805(20)$, meaning the equality is satisfied to one standard deviation.

Another class of relations between critical exponents is given by the hyperscaling relations [43], where the dimensionality of the system enters explicitly. While they take the form of inequalities [47], current results suggest they saturate. Out of the seven inequalities given in [47], two of them involve the exponent μ , related to percolation with an “external field.” Four of them contain the rarely used exponents δ_r and Δ ($\Delta \equiv \beta + \gamma$). Another relation depends on ν but not on η . The remaining one, dependent on d , is

$$(d - 2 + \eta)\nu - 2\beta \geq 0. \tag{11}$$

With our value of η and using $\beta = 0.41(1)$ [48], one gets $(1 - \eta)\nu - 2\beta = 0.018(22)$, so the left-hand side of (11) is compatible with 0. Applying finite-size scaling to Monte

Carlo simulations gives more precise exponents than renormalization groups techniques, but generally does not give direct access to all exponents. A result of [49], using Eq. (10), is $\eta = -0.04602(34)$, obtained without the use of hyperscaling. This result is compatible with ours within two errors bars. If the hyperscaling equalities could be shown to hold, η could be indirectly determined by measuring the fractal dimension d_f . The value from [46] presented in Table I comes from the relation $\eta = 2 + d - d_f$ and the value $d_f = 2.52293(10)$, which is compatible with our results within two standard deviations. A summary of the various results is presented in Table I, where we also recall in the caption how scaling relations are used to determine η .

VII. CONCLUSIONS

We have constructed a purely geometric theory of percolation, the geometric model *par excellence*, at criticality. The spatial distribution of the giant cluster between the boundaries of the critical system has been linked to the solution of an equation for a metric with constant negative curvature. By using its solutions and results from numerical simulations of continuum percolation, we determined the anomalous dimension η . The fact that our results reproduce the known 2D result and compare favorably with previous determination of η in three dimensions (Table I) is an additional piece of evidence in favor of the critical geometry approach. The hyperscaling equalities with the obtained value of η are shown to be satisfied. The order parameter profile could also be extracted from *lattice* (site or bond) percolation at criticality and then fitted with the solution of the Yamabe equation. We expect that critical exponents would be determined with lower precision with respect to the present results, but it could be suited for larger dimensions $d = 4, 5, 6$ due to the lower numerical effort to generate points and determine cluster formation.

This work opens the possibility to study two- and higher-point correlation functions in percolation, as done for the Ising and the XY model in [29,37]. Further investigation is required to understand how this theory can describe fields other than the order parameter, correlations of different fields, and boundary-condition-changing operators.

ACKNOWLEDGMENTS

G.G. is supported by the Deutsche Forschungsgemeinschaft (DFG, German Research Foundation) under Germany's Excellence Strategy EXC 2181/1-390900948 (the Heidelberg STRUCTURES Excellence Cluster). G.G. also acknowledges QSTAR for hospitality during completion of this work.

APPENDIX A: SOLUTION OF THE FRACTIONAL YAMABE EQUATION

The fractional Yamabe equation used in the main text to obtain the order parameter profile relies upon the consistent definition of a conformally covariant fractional laplacian $(-\Delta)^s$ where $s = \frac{d}{2} - \Delta_\phi$. Since this construction in the domain Ω will be performed for an arbitrary metric g we introduce the new symbol $\mathcal{L}_g^{(s)}$ for the fractional conformal Laplacian while we use $(-\Delta)^s$ just when g is the flat metric.

This is achieved by viewing the domain under consideration Ω , equipped with a metric g , as the boundary of a $(d + 1)$ -dimensional manifold $X = [0, \pi/2] \times \Omega$ endowed with a metric g_+ . In this enlarged space a solution for an eigenvalue problem is searched; this technique has been mathematically introduced in [36] for a compact domain Ω . For a domain with boundary this procedure has to be adapted in the following way. Denoting by $\theta \in [0, \pi/2]$ the extension direction the metric should take the form of a so-called cornered hyperbolic metric [54]:

$$g_+ = \frac{1}{(\sin \theta)^2} (d\theta^2 + g_\theta), \quad (\text{A1})$$

where $g_{\theta=0} = g$ such that on the surface $\theta = 0$, to be identified with our original domain Ω , we have $g_+ \approx \theta^{-2}(d\theta^2 + g)$ making it an asymptotically hyperbolic metric. Moreover g_+ has to satisfy the following conditions:

$$\begin{aligned} \text{Ric}(g_+) + d g_+ &= 0 \\ \partial_\theta g_\theta|_{\theta=\pi/2} &= 0 \\ g_\theta^{-1}|_{[0,\pi/2] \times \partial\Omega} &\rightarrow 0, \end{aligned} \quad (\text{A2})$$

where Ric refers to the Ricci scalar curvature in $d + 1$ dimensions. For a discussion of the meaning of these conditions the reader is referred to Appendix B of [29]. Once we have g_+ we set up the following eigenvalue (scattering) problem for the Laplace-Beltrami operator $(-\Delta_{g_+}^{LB})$ relative to g_+ :

$$\begin{aligned} (-\Delta_{g_+}^{LB})U &= \Delta_\phi(d - \Delta_\phi)U \\ U &= (\sin \theta)^{\Delta_\phi} F_I + (\sin \theta)^{d - \Delta_\phi} F_O \end{aligned} \quad (\text{A3})$$

for the function U defined on X . The functions F_I and F_O are regular and give access to the fractional Laplacian as follows: $\mathcal{L}_g^{(s)} f_I = c_s f_O$ where $c_s = 2^{2s} \frac{\Gamma(s)}{\Gamma(-s)}$, $f_I = F_I|_{\theta=0}$, and $f_O = F_O|_{\theta=0}$.

For the relevant three-dimensional slab geometry the cornered metric satisfying (A1) and (A2) has been obtained in the form:

$$g_+ = \frac{d\theta^2 + dx^2/\gamma_x(x, \theta)^2 + (dy^2 + dz^2)/\gamma_\parallel(x, \theta)^2}{(\sin \theta)^2}. \quad (\text{A4})$$

The functions γ_x and γ_\parallel are plotted in Fig. 6.

Given g_+ , the nonlinear eigenvalue problem

$$(-\Delta)^{d/2 - \Delta_\phi} \gamma_{(\Delta_\phi)}(\mathbf{x})^{-\Delta_\phi} \propto \gamma_{(\Delta_\phi)}(\mathbf{x})^{-d + \Delta_\phi} \quad (\text{A5})$$

implying the solution of (A3) has been tackled numerically, resorting to a variational formulation yielding the desired solution for the fractional Yamabe problem in the slab. For further information the reader is addressed to Appendix C of [29].

Results of this analysis are shown in Fig. 7 for the range of anomalous dimensions $\Delta_\phi \in [0.46, 0.5]$, that is, $\eta \in [-0.04, 0]$ relevant for three-dimensional percolation. In turn this means that we are solving a problem involving a Laplacian raised to a power $s \approx 1.02$ greater than 1. This is to be contrasted with the usual appearance of the fractional Laplacian $(-\Delta)^s$ that has $s \in [0, 1]$. Our numerical framework appears not to be affected by this fact. Note that the small (in the 2×10^{-3} range) deviations from the integer

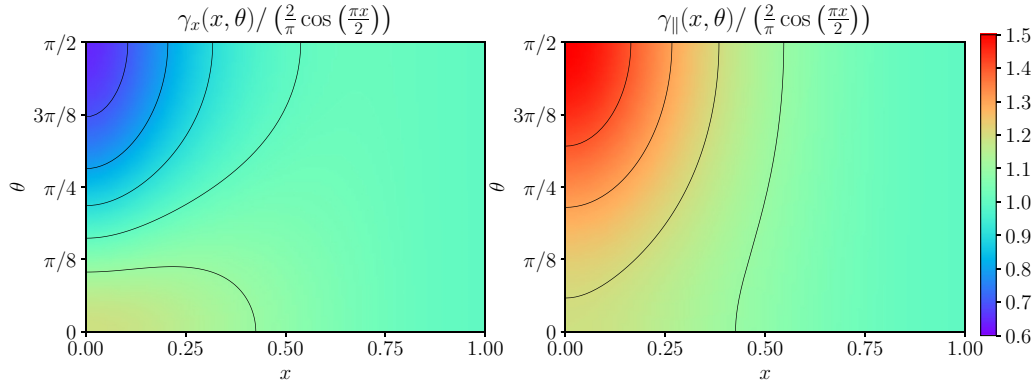


FIG. 6. Functions defining the metric (A4) in the extension space above the slab. The domain shown is $x \in [0, 1]$ (the relevant transverse direction x varies between -1 and 1) and $\theta \in [0, \pi/2]$. The region $x \in [-1, 0]$ can be obtained by reflection. To improve readability, the functions have been divided by $\frac{2}{\pi} \cos(\frac{\pi x}{2})$.

Yamabe problem have been plotted. A list of values of $\gamma_{(\Delta_\phi)}$ for $\Delta_\phi = 0.47846$ is found in Table II.

The solution of the integer Yamabe problem in three dimensions can be written explicitly (as derived in [32]):

$$\gamma_{(\Delta_\phi=1/2)}(x) = \frac{\sqrt{3}}{\omega} \wp\left(\omega\left(1 + i \frac{x}{\sqrt{3}}\right), \{0, 1\}\right), \quad (\text{A6})$$

where $\wp(z, \{0, 1\})$ is the equiharmonic case of the Weierstrass elliptic function with half period $\omega = \frac{\Gamma(1/3)^3}{4\pi}$.

APPENDIX B: DETAILS OF THE SIMULATION

For the sake of clarity, we will describe the algorithm used for the three-dimensional case; the two-dimensional version follows the same concept.

The main difficulty of simulating continuum percolation, compared to the lattice variants [50], is to locate the objects that intersect the newly added one. To do this for the case of spheres, the entire slab has been divided in cubes of size equal to the diameter of a sphere. Since we take the diameter of the spheres to be 1, the number of these boxes will be $N = L \times 4L \times 4L$. Two matrices C and P are then introduced, with N rows and variable number of columns, whose elements

are themselves arrays: they will store, respectively, the coordinates of the sphere centers and a pointer. A new sphere is added by generating the coordinates of its center, uniformly within the slab. From them, we determine to which box it belongs, say, the n th box, which already contained k balls: an array containing the three coordinates is added to $C_{n,k}$, and we also set $P_{n,k} = (-1, 0)$, to signify that the new sphere does not yet belong to any cluster.

Then, we locate all the boxes that could contain spheres intersecting the newly added one: if box n is not on a boundary, we have to check 27 boxes, a $3 \times 3 \times 3$ grid centered in n . For each sphere in one of these boxes, we compute the distance between the two centers: if this is less than the sphere diameter, then an intersection has happened. Now we need to obtain the cluster to which the neighboring sphere belongs, and if it not the same as the cluster of the new sphere, the two will be merged. This is done by a “union/find” algorithm [55]. The idea is to label each sphere so that it points to a sphere in the same cluster. The cluster can then be considered a tree, with various branches growing from one root. The first step is defining a find function: when it is fed the values representing a sphere, (n, k) , it looks at the values in $P_{n,k} = (n', k')$. If n' is negative, by convention, it means that

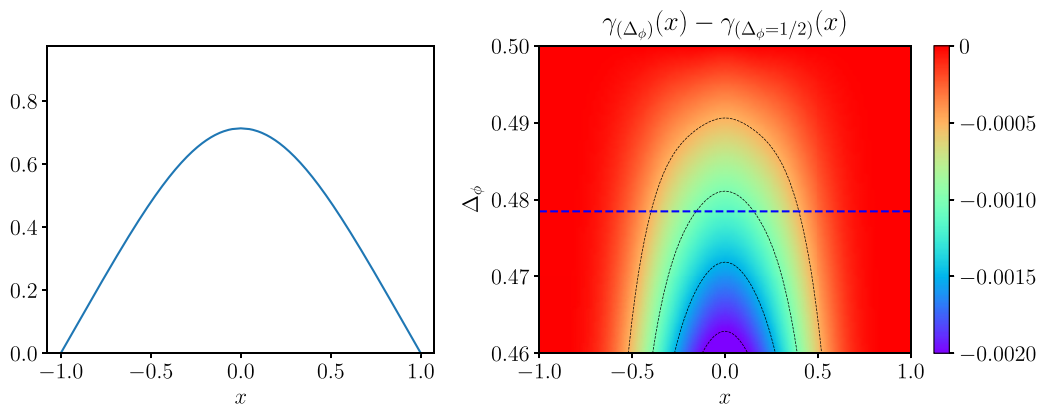


FIG. 7. Solutions of the Yamabe problem in the three-dimensional slab domain ($-1 < x < 1$). Left: Integer Yamabe equation solution (A6). Right: Solutions of the fractional Yamabe equation as Δ_ϕ is varied in the range $[0.46, 0.5]$. The plot shows deviations from the $\Delta_\phi = 1/2$ integer Yamabe solution (in the left panel). The blue dashed line is our best estimate as derived, $\Delta_\phi = 0.47846$.

TABLE II. Values of the solution of the fractional Yamabe equation on the left half of a slab for some values of the coordinate x and $\Delta_\phi = 0.47846$.

x	$\gamma(x)$
-1	0
-0.9	0.099965
-0.8	0.199440
-0.7	0.297174
-0.6	0.391147
-0.5	0.478688
-0.4	0.556675
-0.3	0.621813
-0.2	0.670996
-0.1	0.701632
0	0.712034

the k' 'th sphere in box n' is the root of its cluster. Otherwise, the search continues, as we find the point that (n', k') points to: $P_{n',k'} = (n'', k'')$.

In order to shorten the path for the next time the function is called, once the root is found, the pointer of every sphere along the branch is changed so that it points directly to the root. Next is the “union” part of the algorithm. Once the root of the intersecting sphere is known, if it is the same as the newly added sphere, nothing needs to be done. If the two roots differ, the smaller cluster must be included into the larger one, simply by changing the pointer of its root to the root of the larger cluster. Adding the smaller cluster to the larger one ensures that the average path to the root is shorter, but it might seem that additional effort is required to keep track of the cluster size. However, there is some convenient space to store this information that so far has not been used: the pointer of a root. While the pointer of every other sphere is the location of another sphere, so far we specified only that for a root site (m, q) , $P_{m,q} = (\alpha, \beta)$ with $\alpha < 0$ to distinguish it from other sites. We can set $-\alpha$ to be equal to the number of sites in the cluster and $\beta = 0$ since it does not need to contain any information. Now, when this cluster is merged with another one with root (m', q') and $P_{m',q'} = (\alpha', 0)$, assuming $|\alpha| > |\alpha'|$, we just have to set $P_{m',q'} = (m, q)$ and $P_{m,q} = (\alpha + \alpha', 0)$. This links the smaller cluster to the larger one and updates the size of the latter.

The entire process repeats by adding new balls until the critical filling ratio η_c is reached. The main perk of this algorithm is that each union/find step takes an effectively constant computational time, i.e., it grows extremely slowly with system size. This means that the time to run the entire simulation is, for all practical purposes, simply proportional to the number of balls needed to reach the critical filling fraction.

As previously mentioned, we want to implement fixed boundary conditions. To do so, we add a special object, which is adjacent to all the balls whose center is in a box on either boundary. This ensures that the balls in the first or last layer of boxes all belong to the same cluster, which is then the percolating cluster.

APPENDIX C: DATA ANALYSIS AND TESTS

After obtaining the order parameter profiles, by averaging the results of a few thousand realizations, an additional step is needed before performing the fit. The points closest to the boundary are most affected by finite-size effects. Therefore, despite having smaller errors than the central points, a few of them have to be discarded. In order to determine how many to discard in an unbiased way, as well as to avoid a sharp distinction between discarded and included points, we introduce a window function $w(x)$. The weight of each point in the fit is given by the square of the ratio between this function and the error of that point. This function starts off from 0 at the boundary, ramps linearly to 1 around a movable point t , and maintains the value 1 up to the center of the slab.

To determine the location of the point t , we start from $t = -1$ (the boundary point) and gradually move towards $t = 0$. For each value of t we compute the χ^2 of our data and the corresponding p value. We stop once the p value reaches the reference value $p = 0.95$.

Some more tests are needed to ensure that the errors on the critical filling ratios do not meaningfully affect our results. To that end, we checked that simulations performed at $\eta_c + \sigma_{\eta_c}$ and at $\eta_c - \sigma_{\eta_c}$ give profiles indistinguishable within the error, where σ_{η_c} is the error given in [41] (2D) and [44] (3D). In particular, for small sizes and especially in two dimensions, where σ_{η_c} is very small, varying the number of balls by just one changes the filling ratio from below $\eta_c - \sigma_{\eta_c}$ to above $\eta_c + \sigma_{\eta_c}$. This does not alter the profile and the subsequent Δ_ϕ , either in two or three dimensions.

- [1] D. Stauffer and A. Aharony, *Introduction to Percolation Theory* (Taylor & Francis, London, 2018).
 [2] P. J. Flory, *J. Am. Chem. Soc.* **63**, 3083 (1941).
 [3] W. H. Stockmayer, *J. Chem. Phys.* **12**, 125 (1944).
 [4] G. Caldarelli, R. Frondoni, A. Gabrielli, M. Montuori, R. Retzlaff, and C. Ricotta, *Europhys. Lett.* **56**, 510 (2001).
 [5] P. Grassberger, *Math. Biosci.* **63**, 157 (1983).
 [6] L. Sander, C. Warren, I. Sokolov, C. Simon, and J. Koopman, *Math. Biosci.* **180**, 293 (2002).
 [7] J. C. Miller, *Phys. Rev. E* **80**, 020901(R) (2009).
 [8] J. J. Binney, N. J. Dowrick, A. J. Fisher, and M. E. J. Newman, *The Theory of Critical Phenomena: An Introduction to*

the Renormalization Group (Oxford University Press, Oxford, 1992).

- [9] P. J. Reynolds, H. E. Stanley, and W. Klein, *J. Phys. C: Solid State Phys.* **10**, L167 (1977).
 [10] C.-K. Hu, *Phys. Rev. B* **46**, 6592 (1992).
 [11] R. Rammal and G. Toulouse, *J. Phys. Lett.* **44**, 13 (1983).
 [12] G. Grimmett, *Percolation* (Springer, Berlin, 1999).
 [13] S. Smirnov, *C. R. Acad. Sci. Ser. I Math.* **333**, 239 (2001).
 [14] S. Smirnov, in *Proceedings of the International Congress of Mathematicians, Madrid* (2006), Vol. 2, pp. 1421–1451.
 [15] H. Hinrichsen, *Adv. Phys.* **49**, 815 (2000).
 [16] G. Ódor, *Rev. Mod. Phys.* **76**, 663 (2004).

- [17] M. Aizenman and C. M. Newman, *Commun. Math. Phys.* **107**, 611 (1986).
- [18] M. E. J. Newman, *Phys. Rev. E* **66**, 016128 (2002).
- [19] G. Gori, M. Michelangeli, N. Defenu, and A. Trombettoni, *Phys. Rev. E* **96**, 012108 (2017).
- [20] M. Hu, Y. Sun, D. Wang, J.-P. Lv, and Y. Deng, *Phys. Rev. E* **102**, 052121 (2020).
- [21] B. Nienhuis, in *Phase Transitions and Critical Phenomena*, edited by C. Domb, M. Green, and J. L. Lebowitz (Academic Press, London, 1987), Vol. 11.
- [22] J. L. Cardy, in *Phase Transitions and Critical Phenomena*, edited by C. Domb, M. Green, and J. L. Lebowitz (Academic Press, London, 1987), Vol. 11.
- [23] J. L. Cardy, *J. Phys. A: Math. Gen.* **25**, L201 (1992).
- [24] J. J. H. Simmons, P. Kleban, K. Dahlberg, and R. M. Ziff, *J. Stat. Mech.: Theory Exp.* (2007) P06012.
- [25] J. L. Cardy, [arXiv:9911024](https://arxiv.org/abs/9911024).
- [26] D. J. Amit, D. J. Wallace, and R. K. P. Zia, *Phys. Rev. B* **15**, 4657 (1977).
- [27] P. W. Kasteleyn and C. M. Fortuin, *Phys. Soc. Jpn. J. Supp.* **26**, 11 (1969).
- [28] R. Rattazzi, V. S. Rychkov, E. Tonni, and A. Vichi, *J. High Energy Phys.* **12** (2008) 031.
- [29] G. Gori and A. Trombettoni, *J. Stat. Mech.: Theory Exp.* (2020) 063210.
- [30] A. M. Polyakov, *JETP Lett.* **12**, 381 (1970).
- [31] A. M. Polyakov, *Zh. Eksp. Teor. Fiz.* **66**, 23 (1974).
- [32] A. Galvani, G. Gori, and A. Trombettoni, *Phys. Rev. E* **104**, 024138 (2021).
- [33] H. Yamabe, *Osaka J. Math.* **12**, 21 (1960).
- [34] S.-Y. A. Chang and M. del Mar González, *Adv. Math.* **226**, 1410 (2011).
- [35] M. Kwaśnicki, *Fract. Calc. Appl. Anal.* **20**, 7 (2017).
- [36] C. R. Graham and M. Zworski, *Inv. Math.* **152**, 89 (2003).
- [37] A. Galvani, G. Gori, and A. Trombettoni, *J. High Energy Phys.* **10** (2021) 106.
- [38] F. Kos, D. Poland, D. Simmons-Duffin, and A. Vichi, *J. High Energy Phys.* **08** (2016) 036.
- [39] P. Di Francesco, P. Mathieu, and D. Sénéchal, *Conformal Field Theory*, Graduate Texts in Contemporary Physics (Springer, New York, 1997).
- [40] M. D. Rintoul and S. Torquato, *J. Phys. A: Math. Gen.* **30**, L585 (1997).
- [41] S. Mertens and C. Moore, *Phys. Rev. E* **86**, 061109 (2012).
- [42] G. Gori and A. Trombettoni, *J. Stat. Mech.: Theory Exp.* (2015) P07014.
- [43] J. L. Cardy, in *Scaling and Renormalization in Statistical Physics*, Cambridge Lecture Notes in Physics (Cambridge University Press, Cambridge, 1996).
- [44] C. D. Lorenz and R. M. Ziff, *J. Chem. Phys.* **114**, 3659 (2001).
- [45] J. Adler, Y. Meir, A. Aharony, and A. B. Harris, *Phys. Rev. B* **41**, 9183 (1990).
- [46] X. Xu, J. Wang, J.-P. Lv, and Y. Deng, *Front. Phys.* **9**, 113 (2014).
- [47] H. Tasaki, *Commun. Math. Phys.* **113**, 49 (1987).
- [48] A. Sur, J. L. Lebowitz, J. Marro, M. H. Kalos, and S. Kirkpatrick, *J. Stat. Phys.* **15**, 345 (1976).
- [49] H. G. Ballesteros, L. A. Fernández, V. Martín-Mayor, A. M. Sdupe, G. Parisi, and J. J. Ruiz-Lorenzo, *J. Phys. A: Math. Gen.* **32**, 1 (1999).
- [50] C. D. Lorenz and R. M. Ziff, *Phys. Rev. E* **57**, 230 (1998).
- [51] N. Jan and D. Stauffer, *Int. J. Mod. Phys. C* **09**, 341 (1998).
- [52] J. A. Gracey, *Phys. Rev. D* **92**, 025012 (2015).
- [53] M. Borinsky, J. A. Gracey, M. V. Kompaniets, and O. Schnetz, *Phys. Rev. D* **103**, 116024 (2021).
- [54] S. E. McKeown, *J. Geom. Anal.* **29**, 1876 (2019).
- [55] M. E. J. Newman and R. M. Ziff, *Phys. Rev. E* **64**, 016706 (2001).